Australian Journal of Basic and Applied Sciences, 5(3): 96-107, 2011
ISSN 1991-8178

Analysis of SAR Levels in Human Head Tissues for Four Types of Antennas with Portable Telephones

[1,2]Mohammad Rashed Iqbal Faruque, [1]Mohammad Tariqul Islam, [1,2]Norbahiah Misran

[1]Institute of Space Science (ANGKASA),
[2]Dept. of Electrical, Electronic and Systems Engineering,
Faculty of Engineering and Built Environment,
Universiti Kebangsaan Malaysia, 43600 UKM, Bangi, Selangor, Malaysia.

Abstract: In this paper, a comparative study of several antennas commonly used in portable telephones is investigated. These include a monopole, a helix, a patch and a PIFA antenna. Each one of these structures is modeled and numerically tested using finite-difference time-domain (FDTD) method by using CST Microwave Studio. The testing procedure involves antenna simulation in the proximity of the human head and hand. The behavior of each antenna is evaluated for variable distances from the head geometry (0 - 20 mm). The simulation outputs used as measures for this comparative study include the specific absorption rate (SAR). The computed SAR levels within each of the considered tissues vary for the four antennas under investigation and are within the determined health safety standards. Results suggest that the patch antenna may be the structure of choice when considering safety standards, as its radiation yields the lowest local SAR in the head tissues.

Key words: FDTD method, helix antenna, monopole antenna, portable telephones radiation, PIFA antenna, patch antenna, safety standards, SAR

INTRODUCTION

Interaction of handset antennas with human body is a great consideration in cellular communications. The user's body, especially head and hand, influence on the antenna voltage standing wave ratio (VSWR), gain and radiation patterns. Furthermore, thermal effect, when tissues exposed to unlimited electromagnetic energy, can be a serious health hazard. So standard organizations have set exposure limits in terms of the specific absorption rate (SAR) [ICNIRP (International Commission on Non-Ionizing Radiation, 1988; IEEE Std C95.1-2005; 2005).

Simplified phone antennas such as half-wavelength dipoles in free space or quarter-wavelength monopoles mounted on a metallic box have been frequently investigated in the literature. At the present time PIFA and helical antennas are two commonly used handset antennas. Today, the handset antennas are designed to be able to support two or more frequency bands of various cellular networks. It is required to perform a comprehensive study to determine which handset antenna has better performance and less health hazard. Also it is needed to determine which frequency band is better for operation (Yoshida *et al*., 2005; Kiminami *et al*., 2005; Jensen *et al*., 1995).

In one of the first investigations in this area (Jensen *et al*., 1995), a comparative study has been performed among a monopole antenna and some different types of single band PIFA antennas. Size of the investigated antennas and length of handset boxes used in (Jensen *et al*., 1995) are considerably greater than those used today. SAR and temperature rise in a human head have been calculated for electromagnetic radiation from a monopole, single band helix, and side mounted single band PIFA antenna at 900 MHz and 1800 MHz (Vorst *et al*., 2006). Effect of the separation distance between the antenna and user head has been studied for a dual band PIFA handset antenna (Saraereh *et al*., 2004). This study has shown that there is a proportional relation between SAR and antenna efficiency. In (Jin *et al*., 2005), SAR induced in a cubic head model by two single band helical antenna, one radiates at 900 MHz and the other radiates at 1800 MHz, has been calculated and the effect of mobile shell material has been studied. SAR and radiation efficiency has been measured for four types of PIFA designed for the PCS frequency band (1850 MHz– 1990 MHz) and it has been shown that handsets with higher-efficiency antennas might not necessarily have higher total radiated power due to the SAR

Corresponding Author: Mohammad Tariqul Islam, Institute of Space Science (ANGKASA)

limit (Li and Rahmat-Samii, 2005). The head loss for twenty different mobile phones, with external and built-in antennas, has been measured (Kildal and Carlson, 2002). The measured results have been compared; it has been shown that the handsets with built-in antennas are much less sensitive to how the phone is held than the handsets with external antennas. In (Kouveliotis *et al*., 2006), interaction of a single band helical antenna, mounted on a metallic box, with a human spherical head model has been investigated and reported. SAR level in head from a monopole, a helix, and a PIFA antenna at 1.8-2.2 GHz has been computed and it has been shown that the PIFA antenna produces the lowest SAR in the head tissues (Stevens and Martens, 2000; Ebrahimi-Ganjeh and Attari, 2007; Kuo *et al*., 2007). For a helical antenna operating at 900 MHz, the SAR quantity, radiation patterns and radiation efficiency in the presence of human head and hand has been computed (Ebrahimi-Ganjeh and Attari, 2007). In another investigation, interaction of a dual band gap loop antenna with human head and hand has been investigated (Kuo *et al*., 2007).

IEEE Standard 1528 and IEC 62209-1 specify protocols and process for the measurement of the peak spatial-average specific absorption rate (SAR) induced inside a simplified model of the head of the users of hand held radio transceivers (cellular phones). For example, the SAR limit specified in IEEE C95.1: 1999 is 1.6 W/Kg in a SAR 1 gm averaging mass while that specified in IEEE C 95.1: 2005 has been updated to 2 W/Kg in a 10 gm averaging mass. This new SAR limit specified in IEEE C 95.1: 2005 is comparable to the limit specified in the International Commission on Non-Ionizing Radiation Protection (ICNIRP) guidelines (ICNIRP (International Commission on Non-Ionizing Radiation, 1988; IEEE Std C95.1-2005., 2005), (Lin, 2000; Yioultsis *et al*., 2002; Kivekas *et al*., 2003; Gabriel *et al*., 1996). Especially, the U.S. Federal Communication Commission (FCC) requires the routine SAR evaluation of phone model prior to device authorization or use since 1997.

It should be noted that similar studies have been reported, but with different antenna types, different antenna sizes, number of irradiated tissue types, different antenna frequency, and lower spatial model used to simulate wave-tissue interaction (Yioultsis *et al*., 2002).

The four types of antennas typically used in cellular telephones: monopole, helix patch and PIFA antenna has been selected for this research. Antennas under investigation have different radiation patterns and hence result in different SAR levels in the head tissues. We compare the power deposition with respect to the SAR levels to determine the antenna that best complies with the safety standards. The following antennas are used in the simulation: monopole (Fig. 1), helix (Fig. 2) (Bernadi *et al*., 2001), and the patch (Fig. 3) (Yioultsis *et al*., 2002). and PIFA (Fig.4) (Li and Rahmat-Samii, 2005). All antennas were fed with a 250-mW continuous-waveform source at 1.8-2.2 GHz.

Ii. Physical/computer Modeling:

Ii.a.fdtd Implementation:

The FDTD methodology [2-10] is derived from Maxwell's time-domain equations which may be expressed as

$$\mu \frac{\delta \vec{H}}{\delta t} = -\nabla \times \vec{E}. \tag{1}$$

$$\varepsilon \frac{\delta \vec{E}}{\delta t} = \nabla \times \vec{H} - \sigma \vec{E}. \tag{2}$$

where $\vec{E}$ and $\vec{H}$ are the electric and magnetic field intensities and ε, μ and σ are the space dependent permittivity, permeability, and conductivity, respectively. Using a discretization of the calculus operators in these equations results in a set of algebraic time-stepping relations which may be written in a compact form as

$$\vec{H}^{n+\frac{1}{2}} = \vec{H}^{n-\frac{1}{2}} + \overline{\overline{\gamma}}.\{D_x(-\hat{x}\times\vec{E}^n) + D_y\left(-\hat{y}\times\vec{E}^n\right) + D_z(-\hat{z}\times\vec{E}^n)\}. \tag{3}$$

$$\vec{E}^{n+\frac{1}{2}} = \overline{\overline{\alpha}}.\vec{E}^n + \overline{\overline{\beta}}.\{D_x(\hat{x}\times\vec{H}^{n+\frac{1}{2}}) + D_y\left(\hat{y}\times\vec{H}^{n+\frac{1}{2}}\right) + D_z(\hat{z}\times\vec{H}^{n+\frac{1}{2}})\}. \tag{4}$$

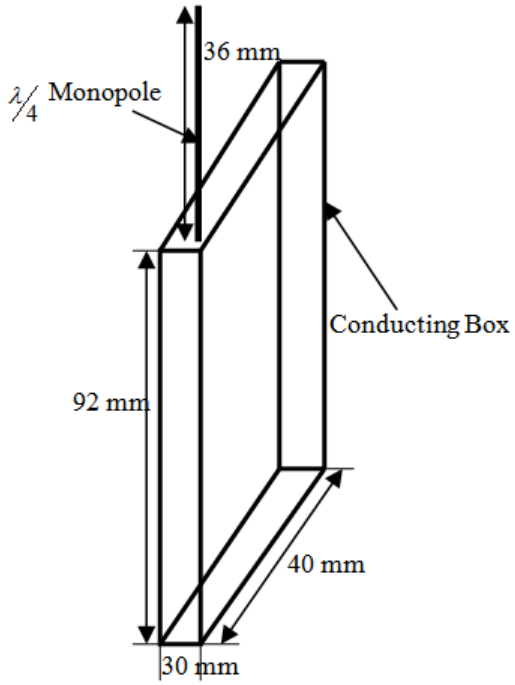

Fig. 1: Monopole antenna. All the dimensions in the sketch are given in millimeters. The monopole is fed with a 250-mW, 1.8-2.2 GHz source and the casing is used to define the ground.

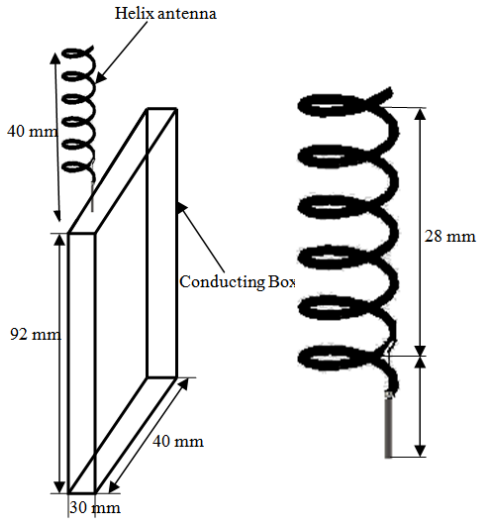

Fig. 2: Helix antenna, adopted from literature with modifications (Bernadi *et al*., 2001). The helix is fed with a 250-mW, 1.8-2.2 GHz source and the casing is used to define the ground. (a) Overall dimensions of the analyzed structure. (b) detailed dimensions of the helix radiating element.

where the superscript denotes the time step t = n Δt and the difference operator is defined as

$$D_x \vec{f}(x,y,z) = \frac{\vec{f}(x+\Delta x/2,y,z) - \vec{f}(x-\Delta x/2,y,z)}{\Delta x}. \quad (5)$$

The terms $\overline{\overline{\alpha\beta}}$ and $\overline{\gamma}$ are space-dependent diagonal tensors whose components are defined by

$$\alpha_{pp} = \frac{\frac{\vec{\varepsilon}_p}{\Delta t} - \frac{\vec{\sigma}_p}{2}}{\frac{\vec{\varepsilon}_p}{\Delta t} + \frac{\vec{\sigma}_p}{2}} \beta_{pp} = \frac{1}{\frac{\vec{\varepsilon}_p}{\Delta t} + \frac{\vec{\sigma}_p}{2}} \gamma_{pp} = \frac{\Delta t}{\vec{\mu}_p} \tag{6}$$

for p =x, y, or z. The symbols characterized by an over bar ($\vec{\cdot}$) represent averaged values of the constitutive parameters over a face of a cell in the discretized computational grid, such as

$$\vec{\varepsilon}_p = \frac{\int_{\Delta S} \varepsilon(\vec{r})\hat{p}.d\vec{S}}{\Delta S}. \tag{7}$$

where ΔS represents the area of the cell face normal to the unit vector p. Using the definitions in (6) and (7) allows accurate modeling of inhomogeneous materials within the computational domain. The relations in (3) and (4) are used to track the time-evolution of the fields in the spatial domain by initially setting all field values to zero. An antenna excitation is then introduced by specifying a voltage at the antenna feed point. The value of the magnetic and electric field intensities are alternately computed at times t= (n+1/2) Δt and t= (n+1) Δt. At grid points coincident with perfect electric conductors, the tangential components of $\vec{E}$ are set to zero at each time step. Special considerations are made for modeling wires and lumped elements within the domain (Jensen *et al*., 1995), and absorbing boundary conditions (Kouveliotis *et al*., 2006) are used to truncate the mesh a reasonable distance from the antenna. Once the time domain data has been collected, a fourier transform is used to obtain the desired frequency-domain quantities such as input impedance, radiation pattern, and gain. In this fashion, the antenna response over a given bandwidth may be obtained.

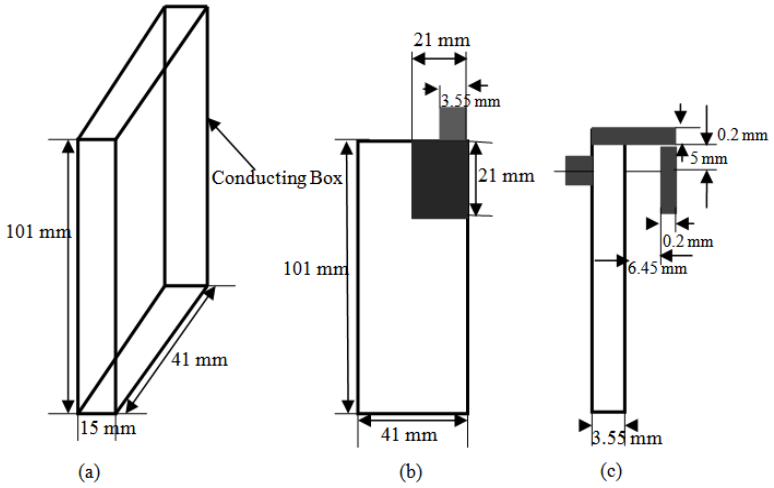

Fig. 3: Patch antenna-All dimensions in the sketch are given in millimeters. The antenna is a modified version on the antenna formerly reported in the literature (Yioultsis *et al*., 2002). (a) The overall telephone casing dimensions. (b) Broad-side view and (c) narrow-side view of the chassis and the patch. The chassis and the patch are embedded within the casing. The chassis is used to define the ground.

The antenna excitation is introduced into the computational domain using a previously reported simulated co-axial feed model (Jensen *et al*., 1995). The functional form of the voltage applied in the feed is a sinusoid modulated by a Gaussian as expressed by

$$S(t) = e^{-(t-t_0)^2/2\sigma_t^2} \cos\left[2\pi f_0 (t-t_0)\right] \tag{8}$$

Where f_0 is the sinusoidal frequency and σ_t controls the pulse width. This particular functional form of interesting since the center frequency and bandwidth of its spectrum may be controlled. In this work, antenna impedance computations over a band are performed using the parameters σ_t =160 ps and f_0 =0. In computing

this transient response, the time-stepping is continued until the antenna current magnitude has decayed to a level approximately 40 dB below its peak value.When computing radiations patterns and power absorption in tissues, a single frequency source is used such that $\sigma_t \infty$. In this case, the time stepping is performed for several cycles (~20) in order for the system to reach a steady state.

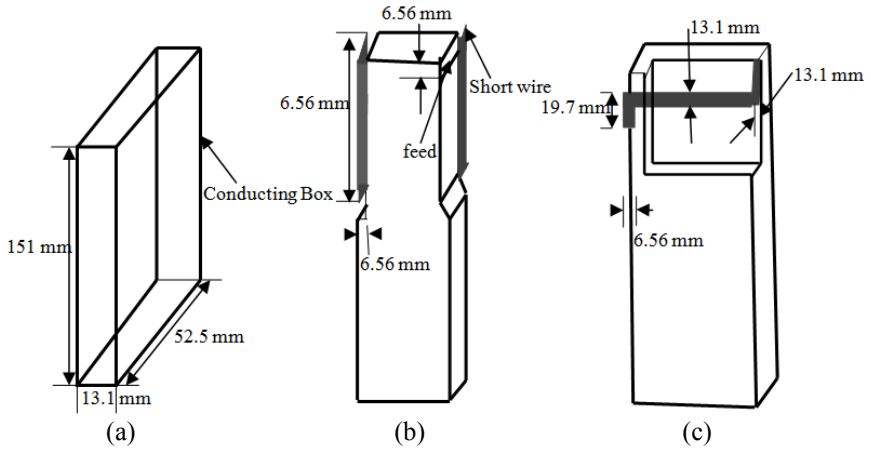

Fig. 4: PIFA antenna-All dimensions in the sketch are given in millimeters. The antenna is a modified version on the antenna formerly reported in the literature (Li and Rahmat-Samii, 2005). The overall telephone casing dimensions.(b) side-mounted dual PIFA and (c) back-mounted PIFA. The chasis dimensions (105 cm3) shown in (a) apply to all three configurations.

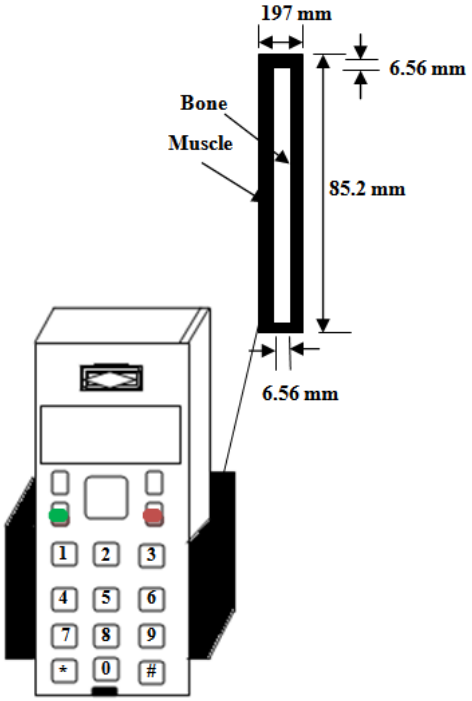

Fig. 5: Block model of the human head used in the simulation of antennas on the handset

Ii.b. Biological Tissue Modeling:

Anatomical human features are modeled within the FDTD framework by mapping the spatial location of the different tissues into a permittivity and conductivity assignment in the computational grid. The human hand is simply modeled as a layer of bones surrounded by a layer of muscles that covers three sides of the handset, as depicted in Fig. 5. To construct a head model, a grid with a 6.56 mm spatial resolution was placed on cross-sectional images of the head obtained from an anatomy atlas (Stevens and Martens, 2000; Bernadi *et al*.,

2001). Magnetic resonance images (MRI) were also used to aid in the tissue classification and location. Each cell in the grid was then assigned a permittivity and conductivity classification corresponding to the type of tissue which fields the majority of the cell. Fig. 5 provides two different views of the head /hand /handset configuration with the dimensions used in the computations. The electrical parameters corresponding to each tissue around the operating frequency of 900 MHz have been obtained from published data are listed in Table 1 (Li and Rahmat-Samii, 2005). Since variations in the conductivity and permittivity values are less than 5% and 1%, respectively. If broadband computations are to be performed where the dispersive nature of the tissues is more significant, then special considerations in the FDTD implementation must be made (Ebrahimi-Ganjeh and Attari, 2007).

Two additional comments are warranted concerning the tissue models presented. First, in order to allow the modeling of very realistic operator/handset configurations, it is important to allow the handset to be rotated such that it is positioned between the operator's mouth and ear. This is accomplished by rotating the positions of each cell in the head model in the y-z plane about the head center and reconstructing the grid based upon these rotated tissue locations (Fig. 6). The fact that the handset remains aligned with the FDTD grid allows accurate modeling of its rectilinear features. Second, when using the models in the computations, different FDTD cell sizes are chosen according to the parameter of interest. For example, it has been found that a cell size of 3.28 mm is required in order to obtain an accurate value of the input impedance. However, for pattern and power absorption characterization, a 6.56 mm cell size may be used. These two cell sizes correspond to approximately 14 and 7 cells per wavelength respectively within the high permittivity tissues at the operating frequency. The head models used in this study was obtained from MRI-based head model through the whole brain Atlas website. Various types of tissues, i.e., air, skin, muscle, fat, bone, cerebrospinal fluid (CSF), brain matter (grey and white), blood, cartilage, vitreous humor, lens, and eye sclera were involved in this model. The electrical properties of tissues were taken from (Kouveliotis *et al*., 2006; Kivekas *et al*., 2003; Gabriel *et al*., 1996; Bernadi *et al*., 2001). Table 1 shows their dielectric properties (Li and Rahmat-Samii, 2005).

Table 1: Human head Tissue properties of materials used for simulation

Serial no.	Tissue	Conductivity σ [S/m]	Permittivity ε_r	Density ρ [g/cm^3]
1	Skin	0.82	43.7	1.00
2	Fat	0.11	6.3	1.00
3	Muscle	1.38	53.5	1.05
4	Bone	0.10	7.3	1.20
5	Tendon	0.10	7.3	1.03
6	Cartilage	0.10	7.3	1.00
7	Blood	1.32	63.3	1.00
8	C. S. Fluid	1.67	62.5	1.02
9	Grey Matter	0.67	47.4	1.05
10	White Matter	0.48	39.4	1.00
11	Humor	1.90	70.0	1.00
12	Lens	0.75	45.0	1.05

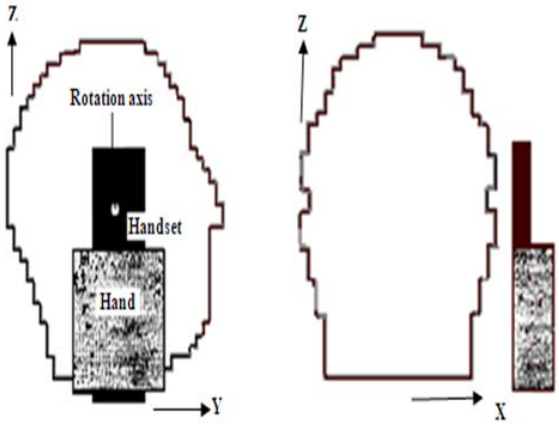

Fig. 6: Slide and rear views of the FDTD head/hand/handset model showing dimensions

***Iii. Methodology and Materials*:**

Antenna radiation and its interaction with the head tissues were simulated with CST Microwave Studio (CST MWS), a three dimensional FDTD numerical tool. Complete handset model composed of the circuit board, LCD display, keypad, battery and housing was used for simulation. The relative permittivity and conductivity of individual components were set to comply with industrial standards. In addition, definitions in (Yioultsis *et al*., 2002) were adopted for material parameters involved in the SAM phantom head. In order to accurately characterize the performance over broad frequency range, dispersive models for all the dielectrics were adopted during the simulation (Kivekas *et al*., 2003; Gabriel *et al*., 1996). The electrical properties of materials used for simulation are listed in Table 2.

Table 2: Electrical properties of materials used for simulation

Phone Materials	ε_r	$\sigma(S/m)$
Circuit Board	4.4	0.05
Housing Plastic	2.5	0.005
LCD Display	3.0	0.02
Rubber	2.5	0.005
SAM Phantom Head		
Shell	3.7	0.0016
Liquid @ 900MHz	40	1.42

CST MWS, which adopted finite difference time-domain (FDTD) proposed by Weiland in 1976, was used as the main simulation instrument In permutation of the perfect boundary approximation (PBA) and thin sheet technique (TST), significant development in geometry approximation with computation speed is achieved squashy highly accurate results. Non-uniform meshing scheme was adopted so that major computation endeavor was dedicated to regions along the inhomogeneous boundaries for fast and perfect analysis.

Fig. 7 shows a heterogeneous realistic head model for FDTD simulation. Numerical simulation of SAR value was performed by FDTD method. The parameters for FDTD computation were as follows. In our lossy-Drude simulation model, the domain were 128 × 128 × 128 cells in FDTD method. The cell sizes were set as $\Delta x = \Delta y = \Delta z = 2.0$ mm. The computational domain was terminated with 8 cells perfect matched layer (PML). The antenna was designed such that the S_{11} response was less than -10 dB over the frequency band of interest. SAM phantom head was then included for SAR calculation using the standard definition as: (Islam *et al*., 2009).

$$SAR = \frac{\sigma}{2\rho} E^2 \quad . \tag{9}$$

where E is the induced electric field (V/m); ρ is the density of the tissue (kg/m^3) and σ is the conductivity of the tissue (S/m). The resultant SAR values averaged over 1 gm and 10 gm of tissue in the head were denoted as SAR 1 gm and SAR 10 gm, respectively. These values were used as a benchmark to appraise the effectiveness in peak SAR reduction.

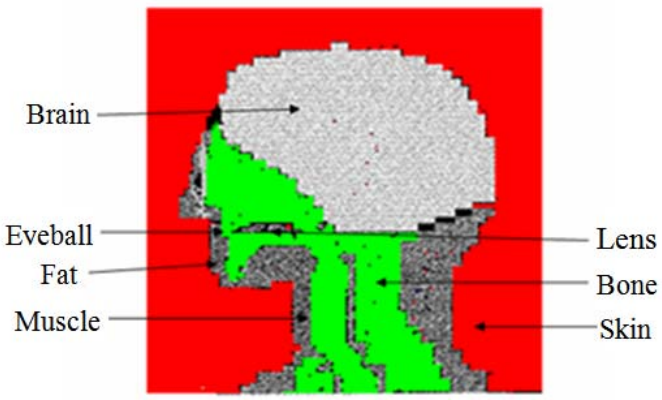

Fig. 7: The heterogeneous, realistic head model for FDTD

RESULTS AND DISCUSSION

The SAR levels for the head tissues are calculated for and with accordance to the two currently accepted standards: FCC and ICNIRP. Continuous waveform, representative of the sources used in mobile telephones, (250 mW, 1.8-2.2 GHz) is used as the form of the antenna excitation. Figs. 8–13 show SAR calculated within the tissues of the human head using the convention of the FCC standard [part (a) of each fig.] and the ICNIRP standard [part (b) of each fig.]. Each graph shows determined maximum average SAR for the volume relevant for the specified standard (1 gm for FCC and 10 gm for ICNIRP) of a particular head tissue as a function of antenna-head distance, for the distance of 0, 2, 4, 6, 8, 10, 12, 14, 16, 18 and 20 mm separating the antenna and the head geometry. In Fig. 8, it is shown that there is a great influence of the distance between the antenna and human head on SAR reduction. If the distance between the antenna and the human head is increased from 0 to 20 mm, then the SAR value also decreases for monopole antenna, from 4.82 to 0.71 W/kg for SAR 10 gm and 14.96 to 1.45 W/kg for SAR 1 gm and also for helix antenna from 2.93 to 0.68 W/kg for SAR 10 gm respectively. It can be seen that for PIFA antenna from 2.02 to 0.58 W/kg and 8.31 to 1.61 W/kg for both cases of SAR 10 gm and SAR 1 gm also decreases. In this fig. it can be observed that the SAR value also decreases for patch antenna from 3.12 to 0.4 W/kg for SAR 10 gm and from 6.31 to 0.88 W/kg for SAR 1 gm. Results are shown for the following tissue types: ear (Fig. 8), skin (Fig. 9), muscle (Fig. 10), skull (Fig. 11), brain—grey matter (Fig. 12) and brain—white matter (Fig. 13). In all graphed results, we observe the expected falloff of the absorbed power with the increased antenna head distance. Nevertheless, with the antenna located very closely to the head, practically all four antenna types exceed the FCC standard within at least one of the tissues under investigation. In particular, the trend demonstrated in all graphs suggests that the monopole antenna is most likely to deposit higher power levels in the head tissues. In comparison, the SAR levels calculated for the patch antenna radiation show that this type of antenna best complies with the safety standards.

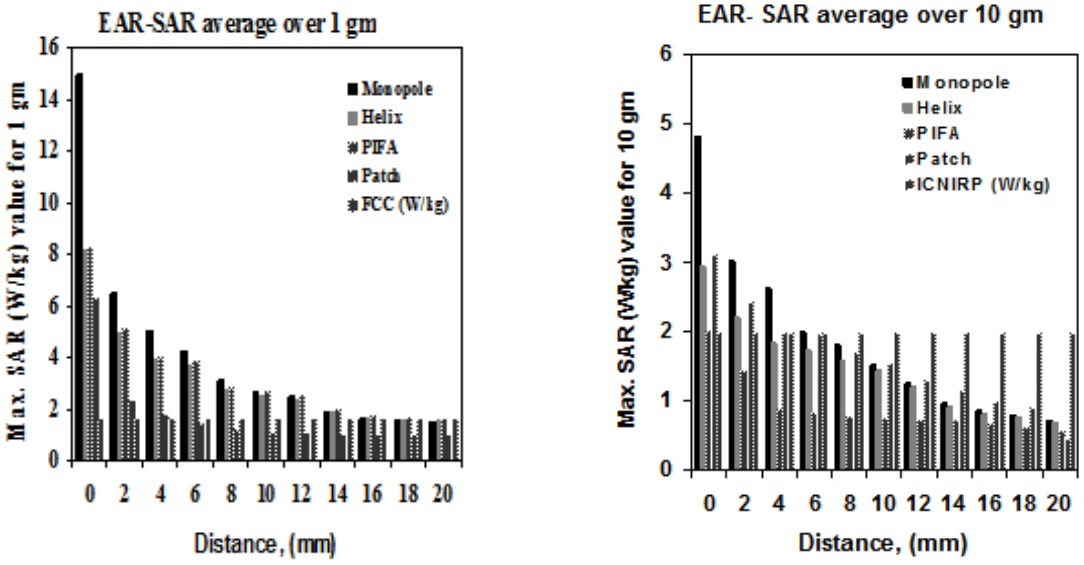

Fig. 8: Maximum SAR averaged over (a) 1 gm and (b) 10 gm of ear tissue as a function of antenna-head distance. Results are shown for four antenna types under investigation: monopole (Fig. 1), helix (Fig. 2), patch (Fig. 3) and PIFA (Fig. 4). Data were calculated for antenna-head distance of 0, 2, 4, 6, 8,10,12,14,16,18 and 20 mm. Safety standard levels determined by FCC (SAR <1.6 W/kg) and ICNIRP (SAR <2 W/kg), are given in (a) and (b), respectively, for reference.

It should be noted that, as expected, the SAR levels differ from one tissue to another. Several factors contribute to this outcome. First, different tissues are located differently with respect to the antenna. Second, electric parameters vary among the tissues, which explicitly affects the SAR, [eqn. (9)]. Since the biochemical processes triggered by an elevated SAR level are dependent on the tissue type (e.g. SAR of 2 W/kg does not carry identical consequences if it occurs in the brain or in the muscle), it is of essence that the power absorption be calculated and assessed for all head tissues separately.

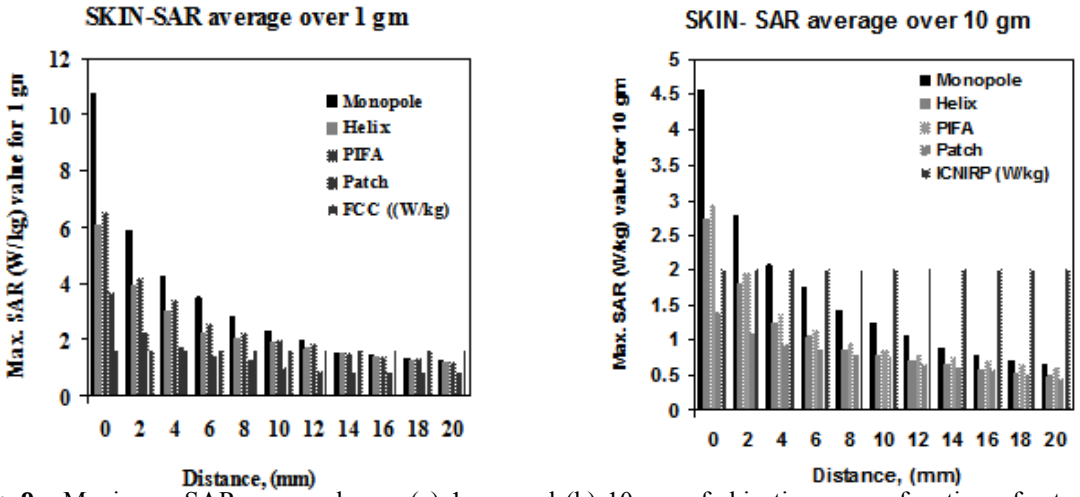

Fig. 9: Maximum SAR averaged over (a) 1 gm and (b) 10 gm of skin tissue as a function of antenna-head distance. Results are shown for four antenna types under investigation: monopole (Fig. 1), helix (Fig. 2), patch (Fig. 3.) and PIFA (Fig. 4). Data were calculated for antenna-head distance of 0, 2, 4, 6, 8,10,12,14,16,18 and 20 mm. Safety standard levels determined by FCC (SAR <1.6 W/kg) and ICNIRP (SAR <2 W/kg), are given in (a) and (b), respectively, for reference.

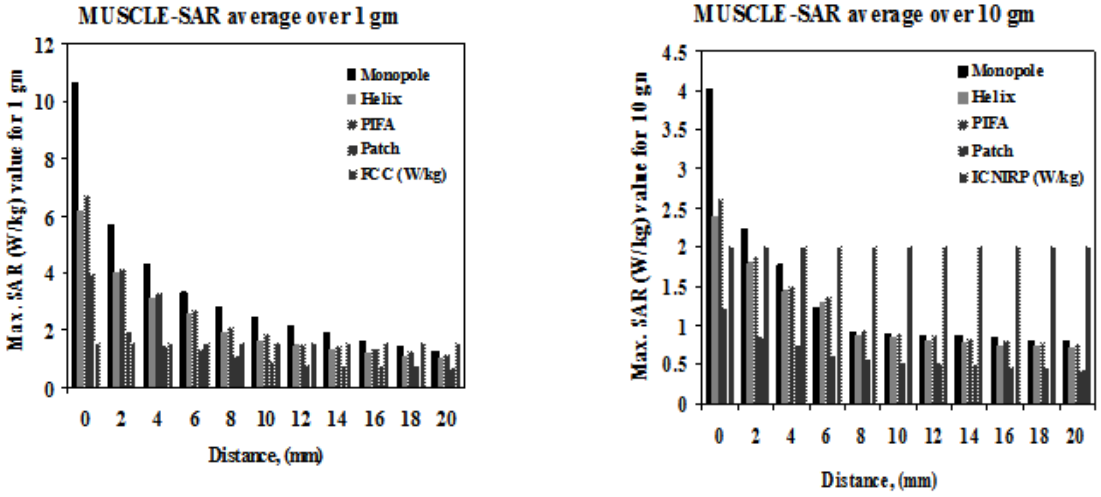

Fig. 10: Maximum SAR averaged over (a) 1 gm and (b) 10 gm of muscle tissue as a function of antenna-head distance. Results are shown for four antenna types under investigation: monopole (Fig. 1), monopole-helix (Fig. 2), patch (Fig. 3.) and PIFA (Fig. 4). Data were calculated for antenna-head distance of 0, 2, 4, 6, 8,10,12,14,16,18 and 20 mm. Safety standard levels determined by FCC (SAR <1.6 W/kg) and ICNIRP (SAR <2 W/kg), are given in (a) and (b), respectively, for reference.

Finally, we would like to stress the impact of the averaging volume (1 gm versus 10 gm) considered for SAR averaging. Figs. 8 – 13 quantify the fact that the ICNIRP more relaxed than the FCC standard. This, however, is not solely due to different absolute maximum SAR threshold values (1.6 W/kg for FCC and 2 W/kg for ICNIRP) but also due to the difference in the test volume of the tissue used for the SAR averaging. The larger volume used by the ICNIRP standard (10 gm) risks to obscure higher SAR values present in the tissue. The FCC standard uses a 1 gm tissue test volume, and, as a result, detects local SAR peaks with better resolution when compared to the ICNIRP. This effect is analogous to the mathematical tools used in image processing to blur images containing visible, sharp contrasts: if the "patch" used for averaging that scans over the image is larger, the more blurred is the resulting processed image.

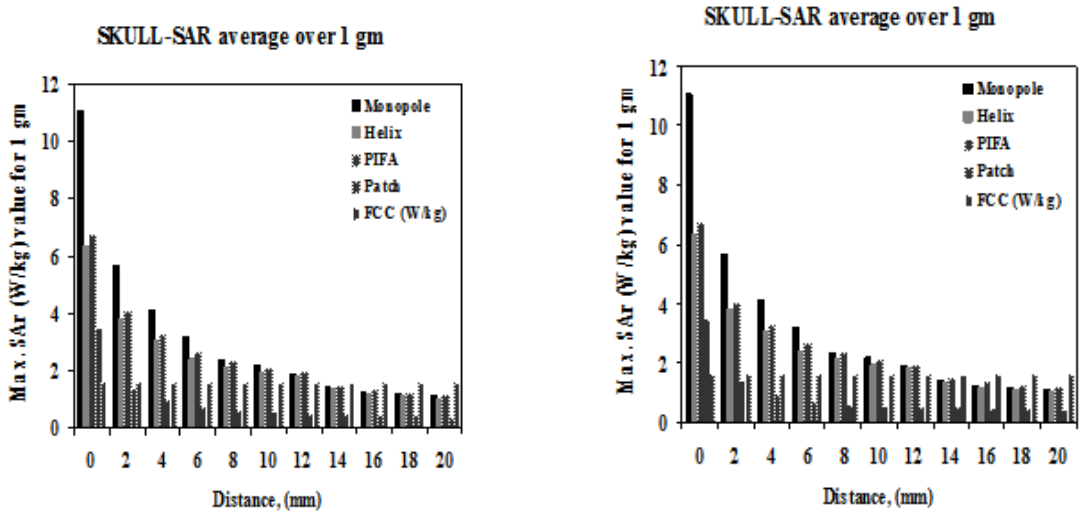

Fig. 11: Maximum SAR averaged over (a) 1 gm and (b) 10 gm of skull tissue as a function of antenna-head distance. Results are shown for four antenna types under investigation: monopole (Fig. 1), monopole-helix (Fig. 2), patch (Fig. 3) and PIFA (Fig. 4). Data were calculated for antenna-head distance of 0, 2, 4, 6, 8,10,12,14,16,18 and 20 mm. Safety standard levels determined by FCC (SAR <1.6 W/kg) and ICNIRP (SAR <2 W/kg), are given in (a) and (b), respectively, for reference.

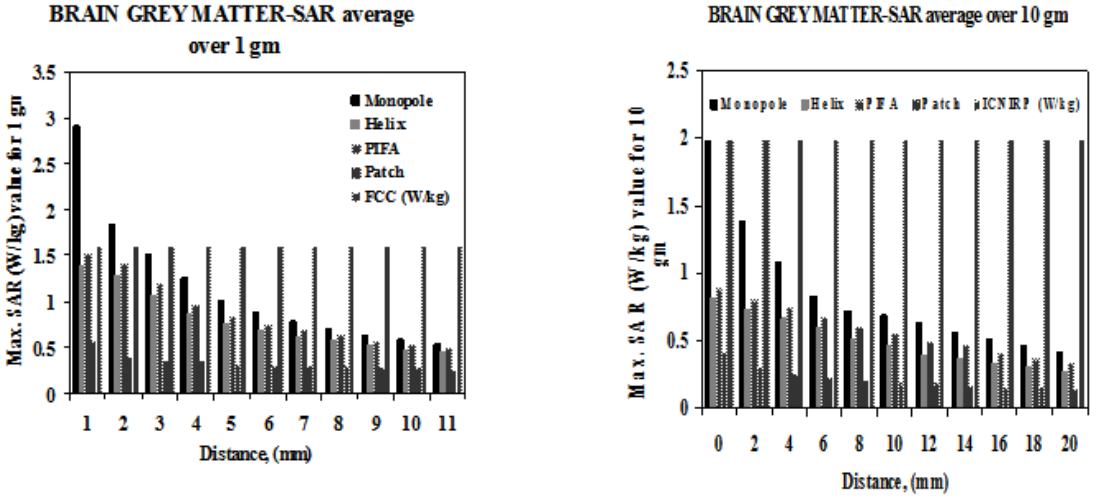

Fig. 12: Maximum SAR averaged over (a) 1 gm and (b) 10 gm of brain tissue (grey matter) as a function of antenna-head distance. Results are shown for four antenna types under investigation: monopole (Fig. 1), helix (Fig. 2), patch (Fig. 3.) and PIFA (Fig.4). Data were calculated for antenna-head distance of 0, 2, 4, 6, 8,10,12,14,16,18 and 20 mm. Safety standard levels determined by FCC (SAR <1.6 W/kg) and ICNIRP (SAR <2 W/kg), are given in (a) and (b), respectively, for reference.

Conclusions:

The comparative study of a monopole, a helix, a patch and a PIFA antenna at 2.2 GHz has been presented in this paper. When the antenna is very close to the human head, all antennas types under study deposit in the near- surface tissues of the head power levels that exceed the FCC standard. The monopole antenna yields the highest SAR levels in all tissues, while the patch is most likely to meet the safety standard. Due to different location with respect to the radiating antenna and different conductivities, not all the tissues experience the same power absorption. SAR must be calculated and averaged separately for each identified tissue volume for accurate and meaningful assessment of potential hazardous implications of the absorbed radiated power.

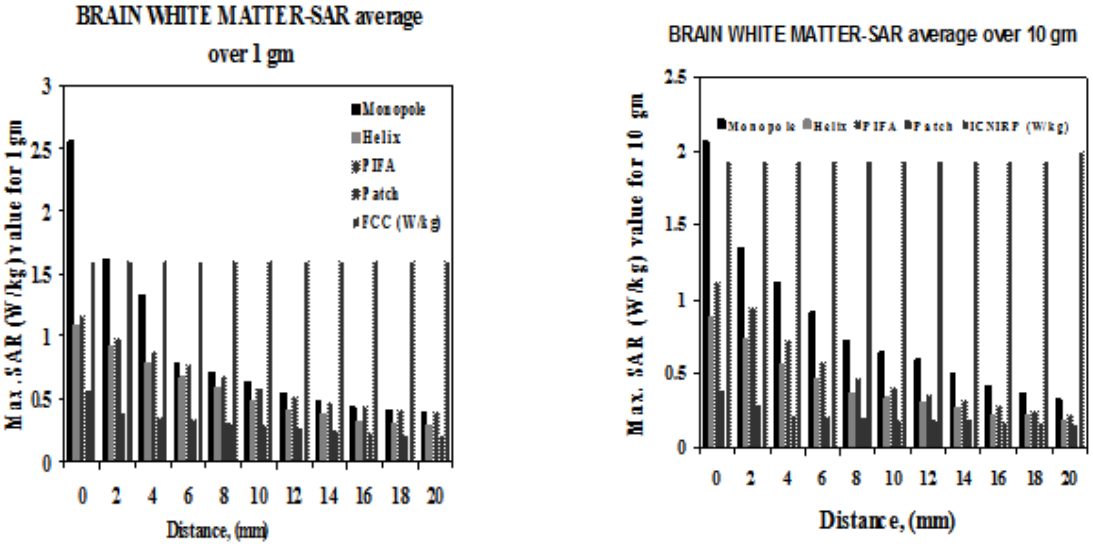

Fig. 13: Maximum SAR averaged over (a) 1 gm and (b) 10 gm of brain tissue (white matter) as a function of antenna-head distance. Results are shown for four antenna types under investigation: monopole (Fig. 1), helix (Fig. 2), patch (Fig. 3.) and PIFA (Fig. 4). Data were calculated for antenna-head distance of 0, 2, 4, 6, 8,10,12,14,16,18 and 20 mm. Safety standard levels determined by FCC (SAR <1.6 W/kg) and ICNIRP (SAR < 2 W/kg), are given in (a) and (b), respectively, for reference

REFERENCES

Bernardi, P., M. Cavagnaro, S. Pisa and E. Piuzzi, 2001. Power absorption and temperature elevations induced in the human head by a dual-band monopole-helix antenna phone, IEEE Transactions on. Microwave Theory and Techniques, 49(12): 2539-2546.

Ebrahimi-Ganjeh, M.A. and A.R. Attari, 2007. Calculation of specific absorption rate (SAR) and studying the radiation performance of the helical antenna, in presence of head and hand model for 900 MHz, presented in 15th Iranian Conference on Electrical Engineering (ICEE2007), Tehran, Iran, May., pp: 15-17.

Gabriel, C., S. Gabriely and E. Corthout, 1996. The dielectric properties of biological tissues: I. Literature survey, Phys. Med. Biol., 41: 2231-2249.

ICNIRP (International Commission on Non-Ionizing Radiation)., 1988. Guidelines for limiting exposure to time varying electric, magnetic, and electromagnetic fields (up to 300 GHz), Health Physics, 74: 494–522.

IEEE Std C95.1-2005., 2005. IEEE standard for safety levels with respect to human exposure to radio frequency electromagnetic fields, 3 kHz to 300 GHz, IEEE New York.

Islam, M.T., M.R.I. Faruque, N. Misran, 2009. Design analysis of ferrite sheet attachment for SAR reduction in human head, Progress In Electromagnetics Research, PIER., 98: 191-205.

Jensen, M.A. and Y. Rahamat-Samii, 1995. EM interaction of handset antennas and a human in personal communication, Proceedings of the IEEE, 83(1): 7-17.

Jin, M., Z. Ying and S. He, 2005. The impact of mobile shell materials on SAR, Asia-Pacific Microwave Conference Proceedings, 5.

Kiminami, K., A. Hirata, Y. Horii and T. Shiozawa, 2005. A study on human body modeling for the mobile terminal antenna design at 400 MHz band, Journal of Electromagnetic Waves and Application, 19(5): 671-687.

Kildal, P.S. and C. Carlson, 2002. Comparison between head losses of 20 phones with external and built in antennas measured in reverberation chamber, IEEE Antennas and Propagation Society International Symposium, 1: 436–439.

Kiveka¨s, O., J. Ollikainen, T. Lehtiniemi and P. Vainikainen, 2003. Effect of the chassis length on the bandwidth, SAR, and efficiency of internal mobile phone antennas, Microwave and Optical Technology Letters, 36(6): 457–462.

Kouveliotis, N.K., S.C. Panagiotou, P.K. Varlamos and C.N. Capsalis, 2006. Theoretical approach of the interaction between a human head model and a mobile handset helical antenna using numerical methods, Progress In Electromagnetics Research, PIER., 65: 309-327.

Kuo, L.-C., Y.C. Kan and H.R. Chuang, 2007. Analysis of a 900/1800-MHz dual-band gap loop antenna on a handset with proximate head and hand model, Journal of Electromagnetic Waves and Application, 21(1): 107-122.

Li, Z. and Y. Rahmat-Samii, 2005. SAR in PIFA handset antenna designs: an overall system perspective, IEEE Antennas and Propagation Society International Symposium, 2B: 784-787.

Lin, J.C., 2000. Specific absorption rates (SARs) induced in head tissues by microwave radiation from cell phones, IEEE Antennas and Propagation Magazine, 42(5): 138-140.

Saraereh, O.A., M. Jayawadene, P. McEvoy and J.C. Vardaxoglou, 2004. Simulation and experimental SAR and efficiency study for a dual-band PIFA handset antenna (GSM 900/DCS 1800) at varied distances from a phantom head, Technical Seminar on Antenna Measurements and SAR (AMS), pp: 5-8.

Stevens, N. and L. Martens, 2000. Comparison of averaging procedures for SAR distributions at 900 and 1800 MHz, IEEE Trans. MTT, 48(11): 2180-2184.

Vorst, A., V.A. Rosen and Y. Kotsuka, 2006. RF/Microwave interaction with biological Tissues, John Wiley.

Yoshida, K., A. Hirata, Z. Kawasaki and T. Shiozawa, 2005. Human head modeling for handset antenna design at 5 GHz band, Journal of Electromagnetic Waves and Application, 19(3): 401-411.

Yioultsis, T.V., T.I. Kosmanis, E.P. Kosmidou, T.T. Zygiridis, N.V. Kantartzis, T.D. Xenos and T.D. Tsiboukis, 2002. A comparative study of the biological effects of various mobile phone and wireless LAN antennas, IEEE Transactions on Magnetics, 38(2): 777-780.